Supplementary information: "Wind waves in sea ice of the western Arctic and a global coupled wave-ice model"

V. T. Cooper[1], L. A. Roach[1*], J. Thomson[2], S. D. Brenner[2], M. M. Smith[2], M. H. Meylan[3] and C. M. Bitz[1]

[1]Department of Atmospheric Sciences, University of Washington, Seattle, WA, USA
[2]Applied Physics Laboratory, University of Washington, Seattle, WA, USA
[3]School of Mathematical and Physical Sciences, The University of Newcastle, Callaghan, NSW 2308, Australia
[*]Now at NASA Goddard Institute for Space Studies and Center for Climate Systems Research, Columbia University, New York City, NY, USA

S1 Attenuation rates in ice

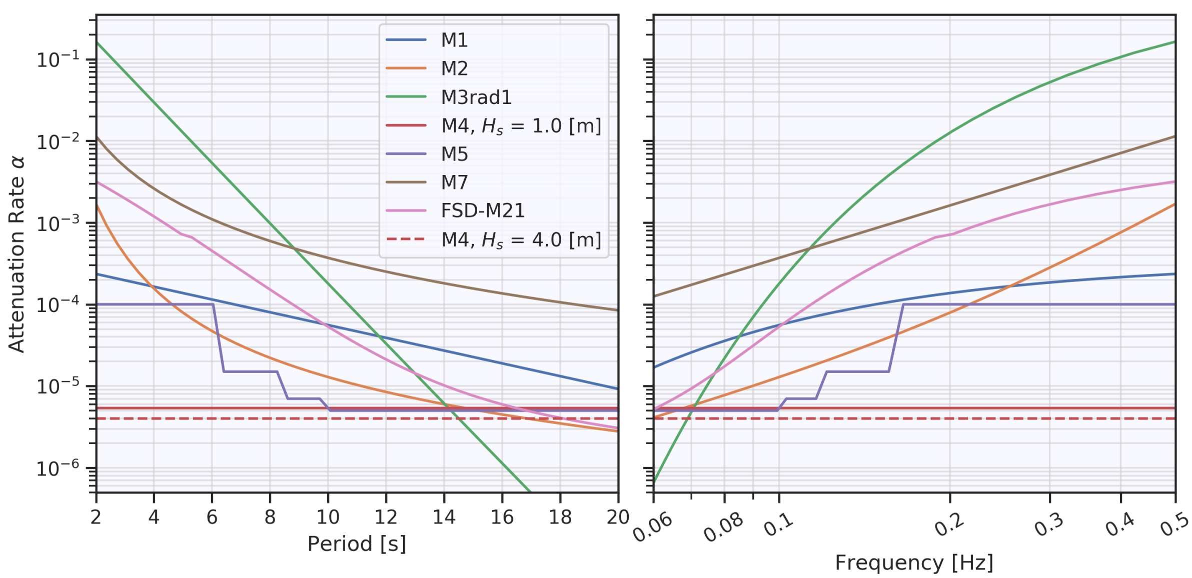

Supplementary Figure 1: Reproduced for reference from [1] based on WW3 model code [2]. Displays the frequency-dependent attenuation rate α of waves in ice used for various experiments corresponding to Table 2 of the main text. For some cases, parameters specified in Table 2 change the α relative to the illustrative values shown here. This plot uses thickness of 0.5 m and, for the FSD-M21 scheme, a floe size of 100 m.

S2 SWIFT surface buoy spectra

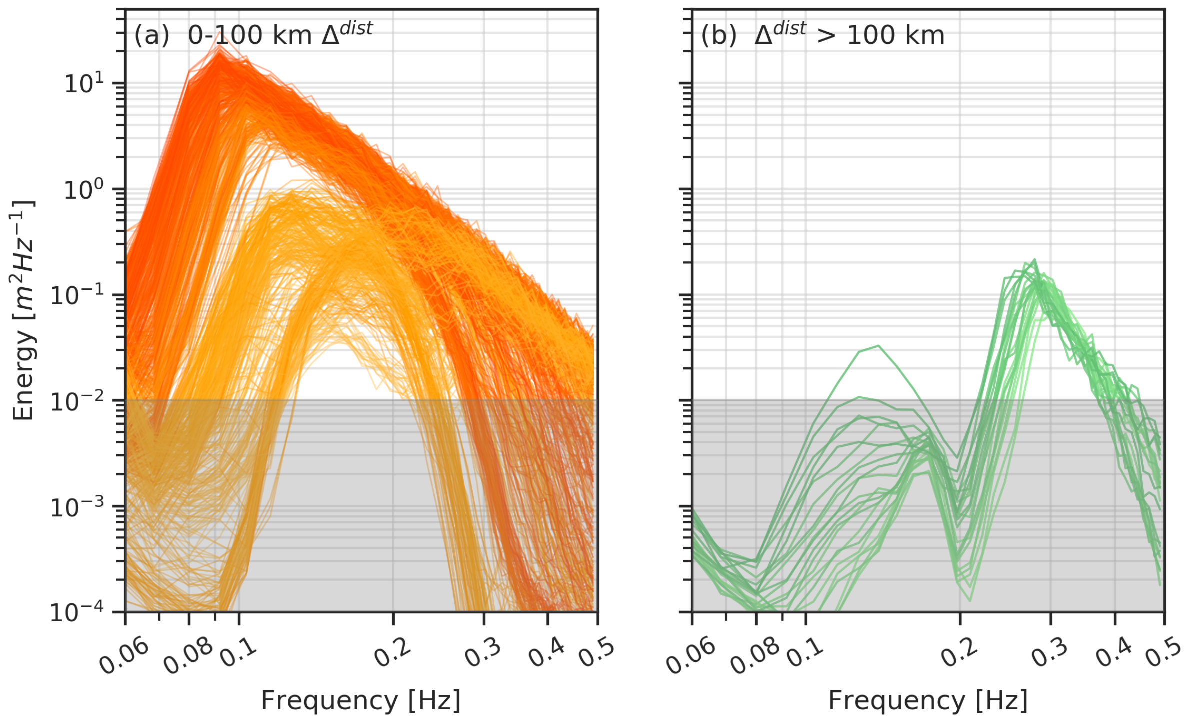

Supplementary Figure 2: Wave spectra from free-drifting surface buoys as a supplemental line of comparison. Color shading according to the peak frequency as visual aid. These measurements come from Surface Wave Instrument Floats with Tracking (SWIFTs) [3] that were deployed for short periods of time during large wave events in the Beaufort-Chukchi Sea during the Oct-Nov 2015 Arctic Sea State campaign. The SWIFTs measure ocean surface velocities and infer wave energy spectra every hour using GPS tracking [4]. The SWIFTs do not sample data continuously over extended periods of time. Only H_s greater than 0.3 m are shown, and the detection limit of the BGOS-SODA observations is marked with grey shading. Note that the SWIFTs have a much lower detection limit, i.e. they resolve the spectra at energy levels much lower than those resolved by the subsurface moorings.

S3 Model spectra in the Beaufort Sea

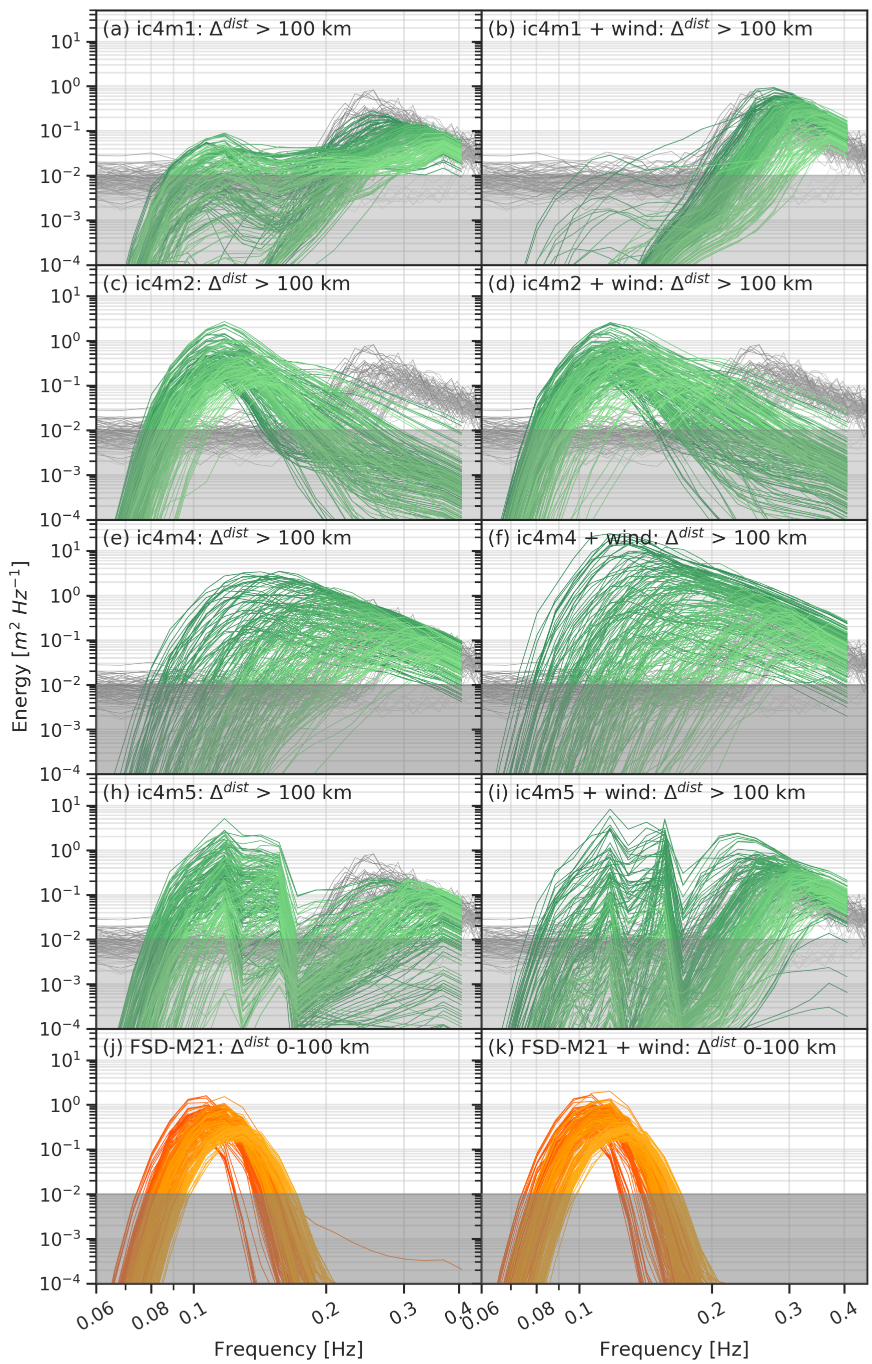

Supplementary Figure 3: A unique random sample of model spectra with description matching Figure 6 of main text.

S4 Timing of BGOS-SODA observations

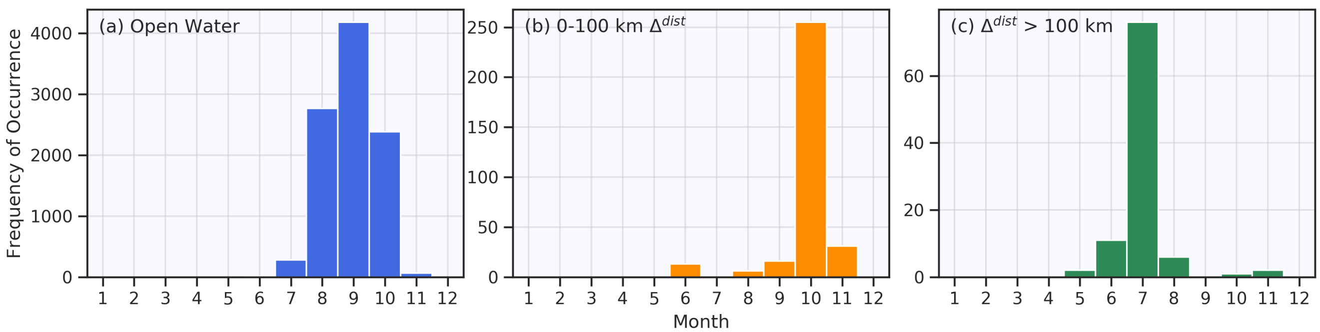

Supplementary Figure 4: Histogram of wave occurrence by month for significant wave height > 0.3 m, spanning 2012-2021 and grouped by Δ^{dist}. Vertical axis represents the number of measurements coming from a given month.

S5 Sea ice concentration: model vs. satellite estimates

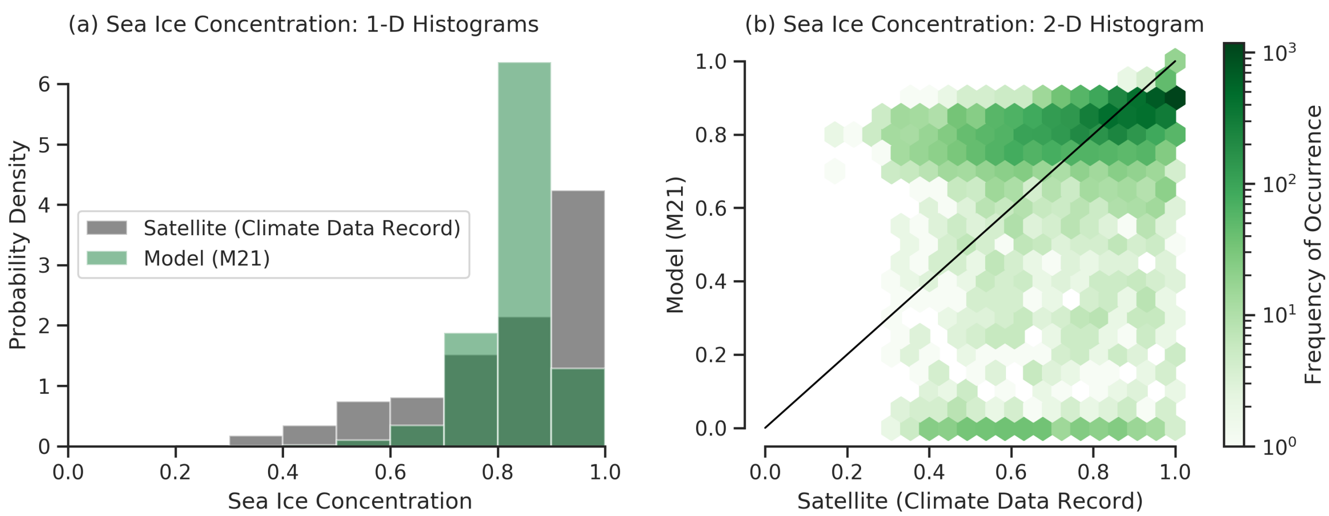

Supplementary Figure 5: (a) Histograms of daily sea ice concentration where $\Delta^{\text{dist}} > 100$ km, during July 2018 for the central Beaufort Sea region surrounding BGOS-SODA observations. NOAA/NSIDC Climate Data Record (CDR) satellite estimates in grey and model output (using the FSD-M21 [5] attenuation scheme and standard wind input) in green. (b) Same data as in a, but represented as a 2-dimensional histogram comparing corresponding grid cells at corresponding times from model output vs. CDR. Note that (a) the model has less probability density in low ice concentrations (e.g. near SIC of 50%) at distances beyond 100 km inside MIZ, and (b) the model tends to have very high SIC (near 80%) when the CDR has intermediate SIC (near 50%).

S6 Model output of sea ice and wave variables (2018)

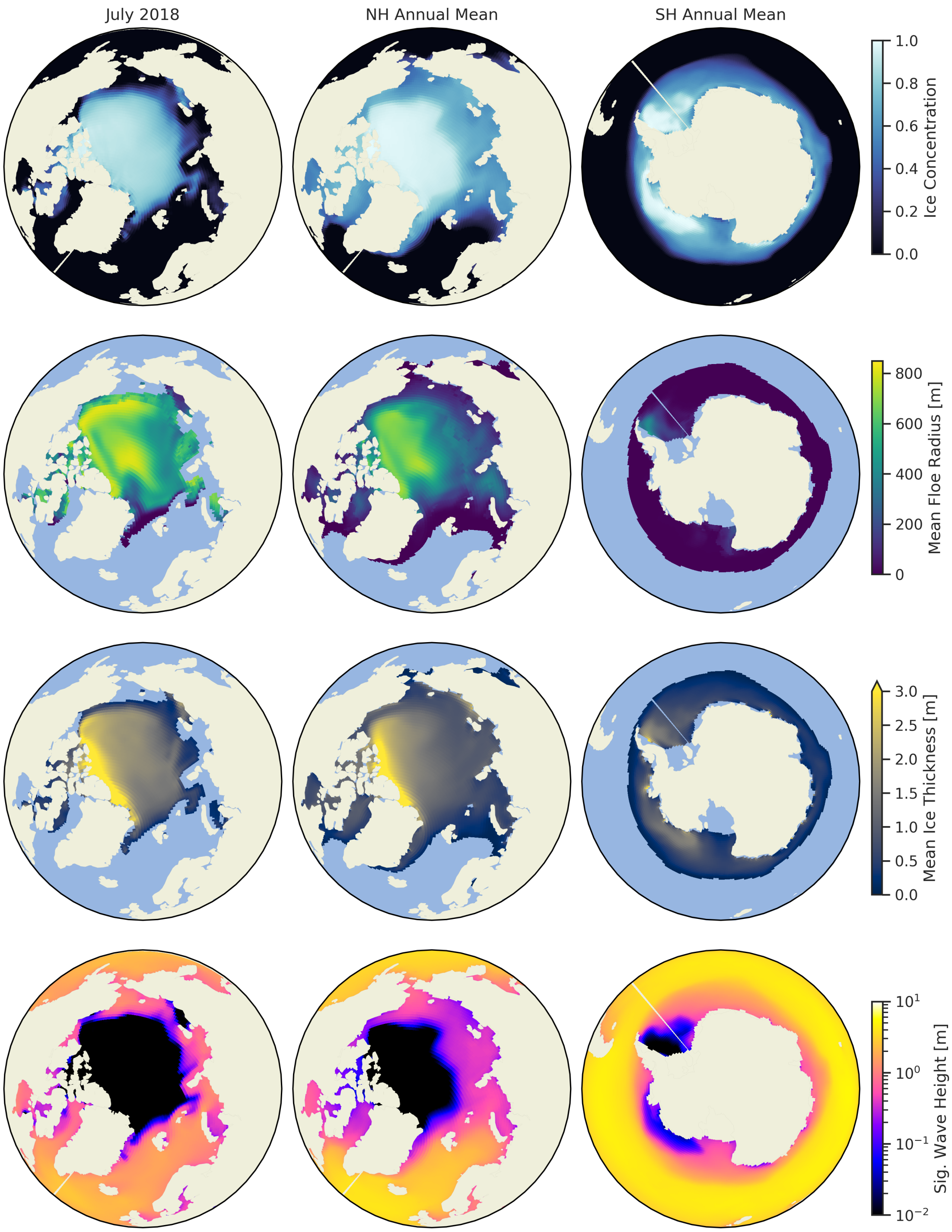

Supplementary Figure 6: July 2018 and 2018 annual mean model output (using FSD-M21 attenuation with standard wind input) for sea ice concentration, mean floe radius, mean ice thickness, and significant wave height. Floe size and ice thickness shown only where ice concentration is greater than 15%.

S7 Floe fracture parameterization applied to observed spectra

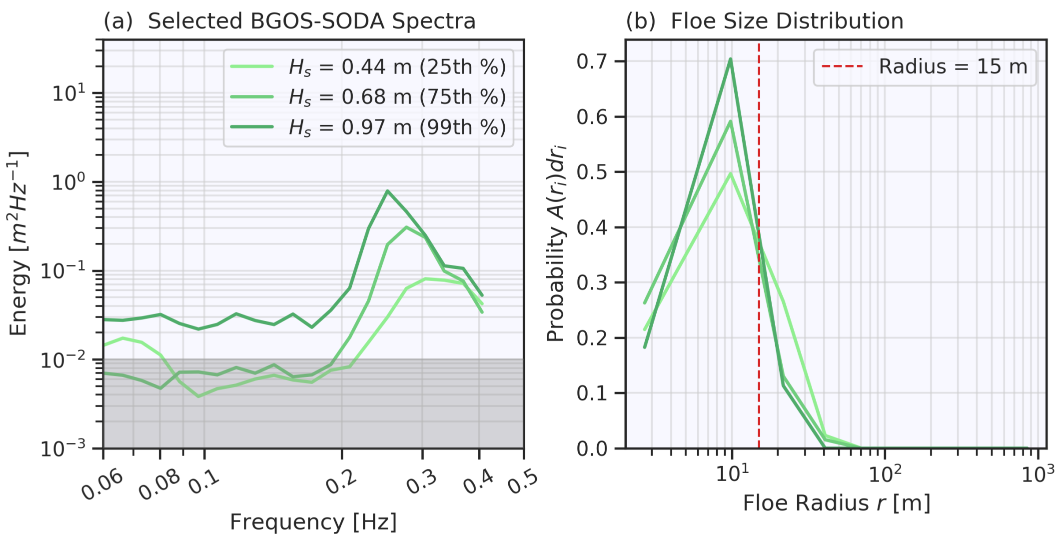

Supplementary Figure 7: (a) Observed spectra from BGOS-SODA at 100+ km Δ^{dist} (25th percentile, 75th percentile, and 99th percentile based on H_s) interpolated to the frequency domain used in model simulations. Grey shading represents approximate detection limit of instruments. (b) Histograms of predicted floe size distributions resulting from fracture by corresponding wave spectra in (a), based on the [6] parametrization, assuming ice thickness of 0.5 m. Floe sizes are binned into probability distributions $A(r)$, where $A(r)dr$ is the fraction of ice area with floe radius between r and $r + dr$. Plots show the probability $A(r_i)dr_i$ at each of the following bin centers i: 3, 10, 22, 41, 70, 114, 176, 260, 370, 506, 668, and 850 m. Red line at radius of 15 m is provided as reference for the limit at which lateral melt has been suggested to be significant [7]

S8 Separation of ice spectra from surface waves and data processing

Supplementary Text: Deformed sea ice produces a "red" spectrum with under-ice topography exhibiting peak spectral variance primarily at low frequencies [8], whereas the surface gravity waves tend to have peak energy in the frequency range of 0.5 to 0.05 Hz, causing sea surface displacements with distinct spectra in that range. Calm waters and smooth ice both produce flat ("white") spectra. If both ice and waves are present, moorings measure a superposition of both signals.

The processing strategies for the mooring datasets make use of these different spectral shapes to identify and separate wave signals from sea ice. The postprocessed wave datasets from BGOS and SODA exclusively contain observations where the surface gravity wave signal is sufficiently strong to be considered a wave, determined by the spectral shape and the total energy in the frequency range of ocean surface waves. If the ice-draft signal is strong while the surface wave signal is weak, the instrument may be unable to produce a valid wave measurement. These instances where only ice draft is detected are excluded from the wave datasets considered here.

Full details of the BGOS data processing are provided in a recent tech report [9]. The report delineates how raw altimeter data are processed into wave spectra following [4, 10, 11] as done in prior studies with BGOS data [12, 13]. Raw data from SODA are quality-controlled using methods comparable to the BGOS methods with details provided in [14].

References

[1] Collins CO, Rogers WE. 2017 A source term for wave attenuation by sea ice in WAVEWATCH III®: IC4 (Tech. Rep. NRL/MR/7320–17–9726). Naval Research Laboratory, Stennis Space Center, MS, USA.

[2] The WAVEWATCH III® Development Group (WW3DG). 2016 User manual and system documentation of WAVEWATCH III® version 5.16. NOAA/NWS/NCEP/MMAB, College Park, MD, USA.

[3] Thomson J. 2012 Wave Breaking Dissipation Observed with "SWIFT" Drifters. *Journal of Atmospheric and Oceanic Technology* **29**, 1866–1882. (doi:10.1175/JTECH-D-12-00018.1)

[4] Herbers THC, Jessen PF, Janssen TT, Colbert DB, MacMahan JH. 2012 Observing Ocean Surface Waves with GPS-Tracked Buoys. *Journal of Atmospheric and Oceanic Technology* **29**, 944–959. (doi:10.1175/JTECH-D-11-00128.1)

[5] Meylan MH, Horvat C, Bitz CM, Bennetts LG. 2021 A floe size dependent scattering model in two- and three-dimensions for wave attenuation by ice floes. *Ocean Modelling* **161**, 101779. (doi:10.1016/j.ocemod.2021.101779)

[6] Horvat C, Tziperman E. 2015 A prognostic model of the sea-ice floe size and thickness distribution. *The Cryosphere* **9**, 2119–2134. (doi:10.5194/tc-9-2119-2015)

[7] Steele M. 1992 Sea ice melting and floe geometry in a simple ice-ocean model. *Journal of Geophysical Research: Oceans* **97**, 17729–17738. (doi:10.1029/92JC01755)

[8] Rothrock DA, Thorndike AS. 1980 Geometric properties of the underside of sea ice. *Journal of Geophysical Research* **85**, 3955. (doi:10.1029/JC085iC07p03955)

[9] Thomson J. 2020 Long-term Measurements of Ocean Waves and Sea Ice Draft in the Central Beaufort Sea. Applied Physics Laboratory, University of Washington.

[10] Kuik AJ, van Vledder GP, Holthuijsen LH. 1988 A Method for the Routine Analysis of Pitch-and-Roll Buoy Wave Data. *Journal of Physical Oceanography* **18**, 1020–1034. (doi:10.1175/1520-0485(1988)018⟨1020:AMFTRA⟩2.0.CO;2)

[11] Thomson J, Girton JB, Jha R, Trapani A. 2018 Measurements of Directional Wave Spectra and Wind Stress from a Wave Glider Autonomous Surface Vehicle. *Journal of Atmospheric and Oceanic Technology* **35**, 347–363. (doi:10.1175/JTECH-D-17-0091.1)

[12] Thomson J, Rogers WE. 2014 Swell and sea in the emerging Arctic Ocean. *Geophysical Research Letters* **41**, 3136–3140. (doi:10.1002/2014GL059983)

[13] Smith M, Thomson J. 2016 Scaling observations of surface waves in the Beaufort Sea. *Elementa: Science of the Anthropocene* **4**. (doi:10.12952/journal.elementa.000097)

[14] Brenner S, Rainville L, Thomson J, Cole S, Lee C. 2021 Comparing Observations and Parameterizations of Ice-Ocean Drag Through an Annual Cycle Across the Beaufort Sea. *Journal of Geophysical Research: Oceans* **126**. (doi:10.1029/2020JC016977)